Cell Reports
Physical Science

CellPress

Article

# Flexible Blue-Light Fiber Amplifiers to Improve Signal Coverage in Advanced Lighting Communication Systems

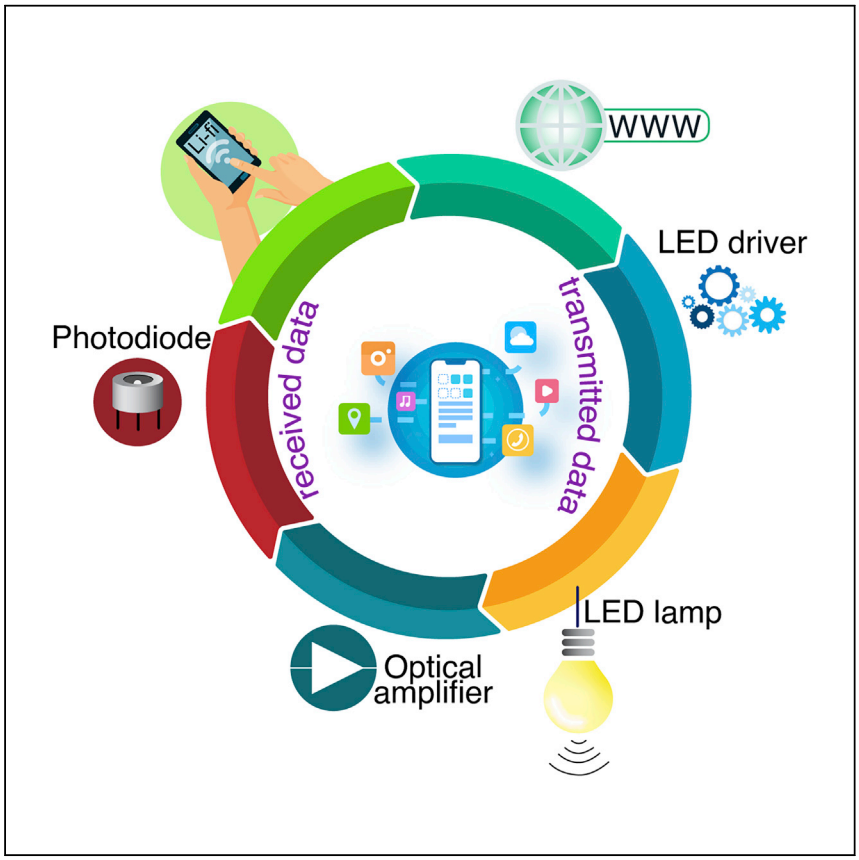


Challenges in visible-light communication (VLC) include mitigation of signal attenuation and fading control. Here, Bastos et al. present a compact and flexible optical fiber amplifier for advanced VLCs and improve the communication reliability demonstrated for pre-amplifier and relay node scenarios and simulated in a realistic environment.

Ana R. Bastos, Guanpeng Lyu, Tiago Silvério, Paulo S. André, Rachel C. Evans, Rute A.S. Ferreira

paulo.andre@istecnico.ulisboa.pt (P.S.A.)
rce26@cam.ac.uk (R.C.E.)
rferreira@ua.pt (R.A.S.F.)

## HIGHLIGHTS

Advanced visible-light communication based on a flexible optical fiber amplifier

Compact optical amplification in pre-amplifier and relay node scenarios

Numerical simulations in realistic environment

Bastos et al., Cell Reports Physical Science 1, 100041
April 22, 2020 
https://doi.org/10.1016/j.xcrp.2020.100041

Cell Reports
Physical Science

CellPress

Article

# Flexible Blue-Light Fiber Amplifiers to Improve Signal Coverage in Advanced Lighting Communication Systems

Ana R. Bastos,[1] Guanpeng Lyu,[2] Tiago Silvério,[1] Paulo S. André,[3,4,*] Rachel C. Evans,[2,5,*] and Rute A.S. Ferreira[1,6,7,8,*]

## SUMMARY

**Visible-light communication (VLC) based on white light-emitting diodes has recently attracted much attention to provide high-bitrate data communication in indoor environments. One of the remaining challenges to be resolved to enable the proliferation of VLC systems is related to channel attenuation and multiple path fading. Here, we introduce an advanced VLC system integrating an optical amplifier as a promising solution to overcome channel impairments, providing high bitrate coverage. The optical amplifier is a flexible fiber based on a poly(fluorene)-based lumophore doped within a di-ureasil organic-inorganic hybrid. Optical amplification is demonstrated for pre-amplifier and relay node scenarios, yielding a maximum gain of 5.9 ± 0.2 dB and 3.7 ± 0.2 dB, respectively, establishing the proposed approach as a promising cost-effective solution for VLCs. Additionally, numerical simulations show, for a realistic environment, a 207% improvement in the coverage area, using existing lighting infrastructure without extra cost.**

## INTRODUCTION

The increasing popularity and rapid development of self-sustainable smart houses and the Internet of Things (IoT) has led to a continuous growth in demand for huge data transmission capacity and multi-functional lighting control from indoor users.[1–3] For instance, it is expected that more than 100 billion IoT devices will support our smart homes and smart cities in the future.[4] Nowadays, digital wireless services are allocated predominantly to the radio frequencies band, which is already congested due to the exponential growth of data traffic, meaning that it is now crucial to look for innovative alternative communication technologies.[5,6] An exciting prospect is visible-light communication (VLC), also known as light fidelity (Li-Fi), which has recently attracted significant attention as a solution to provide high-bitrate data communication in indoor environments.[5] Compared to typical Wi-Fi communication, the VLC system offers unique advantages, such as license-free channels; high electromagnetic immunity; high streaming safety; high modulation bandwidth; a wider region of available frequencies, which can dramatically increase the channel capacity; and the ability to triplicate the number of channels through white light generation by mixing red, green, and blue light.[7–10,12–15] Additionally, because VLC can use existing lighting infrastructure and detection systems, the carbon footprint associated with deployment and manufacturing is low, which may contribute to the achievement of United Nations (UN) sustainable development goals.[16,17] For example, replacement of the 115 million Wi-Fi home spots installed globally in 2017 by VLC could lead to a daily energy saving of 16 GWh,

[1]Phantom-g, CICECO – Aveiro Institute of Materials, Department of Physics, Universidade de Aveiro, 3810-193 Aveiro, Portugal

[2]Department of Materials Science & Metallurgy, University of Cambridge, 27 Charles Babbage Road, Cambridge CB3 0FS, UK

[3]Department of Electrical and Computer Engineering and Instituto de Telecomunicações, Instituto Superior Técnico, Universidade de Lisboa, 1049-001 Lisboa, Portugal

[4]Twitter: @istecnico

[5]Twitter: @LabEvans

[6]Twitter: @ciceco_ua

[7]Twitter: @PhantomG_Aveiro

[8]Lead Contact

*Correspondence: paulo.andre@istecnico.ulisboa.pt (P.S.A.), rce26@cam.ac.uk (R.C.E.), rferreira@ua.pt (R.A.S.F.)

https://doi.org/10.1016/j.xcrp.2020.100041

corresponding to 2.4 million euros per day.[18] Beyond smart buildings, VLC could also have potential in wide-ranging applications, including mobile connection,[19] vehicle-to-vehicle communication,[20,21] underwater resource exploration,[22,23] hospitals,[24,25] and airplane cabins.[26] The commercial potential of this technology is clear, with some forecasts predicting that the global VLC market will be worth up to 90 billion euros by 2024.[27] Several companies (e.g., Target, Emart, and Royal Philips NV) have already implemented a VLC prototype to guide consumers to goods, using light-emitting diodes (LEDs) as data transmitters to communicate with their smartphones.[28]

Currently, LEDs are the light source of choice for data transmission by VLC, due to the ease of modulating the light-intensity at a very fast rate (gigabits per second),[29] which allows them to function both as a light source and wireless signal transmitter. As LEDs have a high market penetration, with the prediction that nearly 75% of all Europe illumination will be provided by LEDs in 2020,[30] VLC can be easily integrated with existing lighting infrastructure, decreasing the deployment cost.[5] LEDs also offer 80% lower energy consumption and 300% higher lifetime than traditional lamps, which is also relevant to meeting UN sustainable development goals.[31] Despite this potential, VLC based on LEDs still needs to overcome some challenges to improve its operational performance, in particular, related to signal attenuation and the multiple optical paths induced by reflections from physical barriers (floor, walls, and objects in the room). In this case, the receiver will collect different signals from optical paths with different propagation delays, causing intersymbol interference, which will decrease the communication reliability.[32] To solve these drawbacks, several solutions have already been proposed. At the transmitter, it is possible to improve VLC by using high-brightness LEDs[33] or light converters (perovskite nanocrystals[34,35] and blends of semiconducting polymers[36]), which exhibit a higher data transmission rate than that of conventional phosphors used in commercial LEDs. At the receiver, the solutions are based on trans-impedance amplifiers,[37] ambient light filtering, and post-equalization techniques in the electronic circuit.[38] Nonetheless, all of these solutions require complete replacement of the infrastructure (LEDs and the photodetectors in computers and smartphones) that is already in place in our society, increasing the deployment cost of VLC technology.

Here, we propose a solution to these challenges based on optical amplification to improve signal quality for direct line-of-sight connection, using current commercial LEDs and photodetectors. To implement this approach, a suitable material that meets the requirements for optical amplification in the visible spectral range must be identified. In addition to exhibiting high optical gain, the material should also have a low absorption coefficient, low power consumption, and be amenable to low-cost production. Organic materials are rapidly emerging as alternatives for applications where inorganics are not ideally suited, such as those requiring large active areas, color tunability, or mechanical flexibility.[39] Due to their high photoluminescence quantum yields ($\phi > 50\%$) and sub-nanosecond emission lifetimes, conjugated polymers (CPs) are attractive candidates for this purpose, because these features enable higher communication bandwidths.[40–42] Nonetheless, morphological control is still a challenge for conjugated polymers, with chain aggregation and entanglements often leading to diminished optical performance.[43] However, we have recently shown that the incorporation of CPs into a di-ureasil organic-inorganic hybrid matrix is an effective approach to minimize interchain interactions leading to highly emissive solid-state materials with high optical gain.[42,44,45] Moreover, the di-ureasil host provides additional features, including enhanced photostability under UV irradiation,[46] intrinsic photoluminescence (PL) in the purple-blue spectral

region with a lifetime of nanoseconds,[47] and materials benefits, such as mechanical flexibility and thermal stability.[48] Di-ureasils are also produced using low-cost solution processing methods, using green solvents and ambient conditions, which are directly translatable to large-scale industrial production. This presents a considerable advantage over classical semiconductors used as optical amplifiers (namely based on the group III–V compound semiconductors), which are fabricated by complex, expensive, and high-temperature physical methods.[49]

Herein, we report a di-ureasil material incorporating the CP, poly[(9,9-dihexylfluorenyl-2,7-diyl)-alt-co-(2-methoxy-5-{2-ethylhexyloxy}-1,4-phenylene)] (PF-MEH) and its implementation as an optical amplifier in a VLC system. PF-MEH is selected as the lumophore due to its high PL quantum yield and emission in the blue spectral region. To optimize implementation in a VLC system, PF-MEH-di-ureasils are processed as free-standing cylindrical fiber monoliths for more efficient coupling with a photodiode, exhibiting a high optical gain. Inspired by this performance, the fibers are tested in a VLC testbed scenario as pre-amplifiers and relay nodes. To demonstrate the reliability of the proposed amplifiers in a more realistic environment, numerical simulations have also been performed to evaluate the performance of the VLC system in a 16-$m^2$ room, using commercial lighting infrastructures based on white light-emitting LEDs.[50]

## RESULTS

### Optical Characterization

Organic-inorganic di-ureasil hybrids incorporating the PF-MEH lumophore at different weight % loadings (0–0.10 wt %; Table S1) were synthesized using the versatile sol-gel process at room temperature and molded as cylindrical fibers (1.5 $\pm$ 0.5 mm diameter and 35.0 $\pm$ 0.5 mm length). The doped PF-MEH-di-ureasil (PF-MEH1–5) fibers all exhibited flexibility, transparency under daylight, and an intense blue emission under UV (365 nm), as shown in Figures 2A–2E.

The parent di-ureasil (dU(600)) shows similar characteristics; however, the observed emission upon excitation at 365 nm is much less intense. The corresponding emission spectrum exhibits a broad band centered between 380 and 450 nm (Figure 2G), which has been previously assigned to radiative electron-hole recombination.[51] The PF-MEH-di-ureasil samples present a broader emission band between 390 and 550 nm (Figure 2G), which is characteristic of the PF-MEH lumophore, with a 4-nm shift when compared to dU(600). As desirable for VLC, the blue emission of the PF-MEH-di-ureasils overlaps with that of the InGaN-based LED used to produce commercial solid-state lighting LEDs, whose white light results from the mixture of the blue emission arising from high-efficiency LEDs and yellow-emitting YAG:Ce phosphor.[50]

The contribution of both dU(600) and PF-MEH excited states to the observed blue emission is also inferred from the excitation spectra monitored around 410 nm (Figure 2F). The spectra are dominated by a band between 250 and 400 nm, assigned to overlapping contributions from PF-MEH and the dU(600) host. However, variations in the relative intensity and bandwidth of the peaks are observed as a function of the PF-MEH wt %, as can be observed between the excitation spectra of the more concentrated samples (PF-MEH3–5) when compared with the low-concentration ones (PF-MEH1–2).

The PL quantum yields obtained on excitation at 365 nm are shown in Table S1 and reveal a significant increase as a function of increasing PF-MEH wt %, reaching a

maximum of 0.519 ± 0.005, observed for PF-MEH5. The dU(600) exhibits a $\phi$ of 0.013 ± 0.001, which is in good agreement with previously reported values.[44] The increase in $\phi$ with concentration shows the significant contribution of the PF-MEH lumophore to the PL as the host exhibits intrinsically lower values. As desired, the enhanced $\phi$ in the blue spectral region makes it easier to excite the samples using commercial UV-emitting LEDs. We note the progress achieved in the last 10 years[52] in the fabrication of compact and higher-output-power UV-emitting LEDs, reinforcing the potential of the material to be integrated with VLC as an optical amplifier.

The optical gain was measured using the variable stripe length technique. Emission spectra were acquired for a stripe length range between 0 and 35 mm. As a representative example, Figure 3A shows the amplified spontaneous emission (ASE) spectra obtained for the PF-MEH3 sample. The ASE spectra for the remaining fibers are illustrated in Figure S1. Figure 3B shows the integrated intensity of ASE versus the stripe length for all samples, with a clear increase in the ASE intensity observed with excitation length, which can be described by the one-dimensional optical amplifier rod model detailed in other studies.[42,53] From the best fit of the data, the optical gain coefficient of the fibers was estimated (Figures 3B and 3C). The gain values increase with lumophore loading in the di-ureasil, as observed in the $\phi$ measurements and for similar materials.[42] The maximum optical gain obtained was 4.9 ± 0.2 dB/cm for PF-MEH5.

### Implementation of Optical Amplifiers in VLC Systems

To further evaluate the PF-MEH-di-ureasil fiber waveguides as optical amplifiers, a VLC system was designed, as shown in Figure 1. A commercial white emission LED lamp was used for illumination and data transmission. As the white emission of the LED is a combination of the faster response time of a blue-emitting LED (peaking at ~450 nm) and a long-lived yellow emission (Figure S2), signal detection and amplification were analyzed in the blue spectral region.

In the pre-amplifier scenario, the fiber output was coupled into the active area of the photodiode and the received signal amplitude was calculated with and without the external UV excitation for different fiber input powers ($0.2 \leq P_{in} \leq 6.1$ mW). The optical gain values were estimated from the ratio between the signal amplitude of the received signal with and without UV excitation. An improvement in the intensity was observed when the external UV source was turned on, yielding a maximum optical gain of 5.9 ± 0.2 dB for PF-MEH5 for an input power of 6.1 mW (Figure 3D). Fibers containing a high PF-MEH loading showed an increase of gain with the input power, with a maximum optical gain observed for sample PF-MEH5, which is consistent with the other optical gain measurements. In contrast, PF-MEH2, which has a low PF-MEH concentration and therefore less optical centers available for excitation, exhibited a saturation regime for input powers higher than 1.0 mW.

Inspired by these results and as a proof of concept, the fibers were also tested as a relay node. In this case, the fiber will amplify and retransmit the signal to the photodiode and is thus placed between the LED lamp and the photodiode. The received signal power was calculated with and without external UV excitation for different powers in the fiber input ($0.1 \leq P_{in} \leq 1.1$ mW). The optical gain values were estimated as detailed above. An improvement in the intensity was observed when the fibers were coupled to the system, yielding a maximum optical gain of 3.7 ± 0.2 dB for PF-MEH5 with a fiber input power of 1.1 mW coupled in the fiber. All fibers presented a linear dependence with the input power at different rates (Figure 3E) due to the different lumophore concentrations in each sample. Comparing both

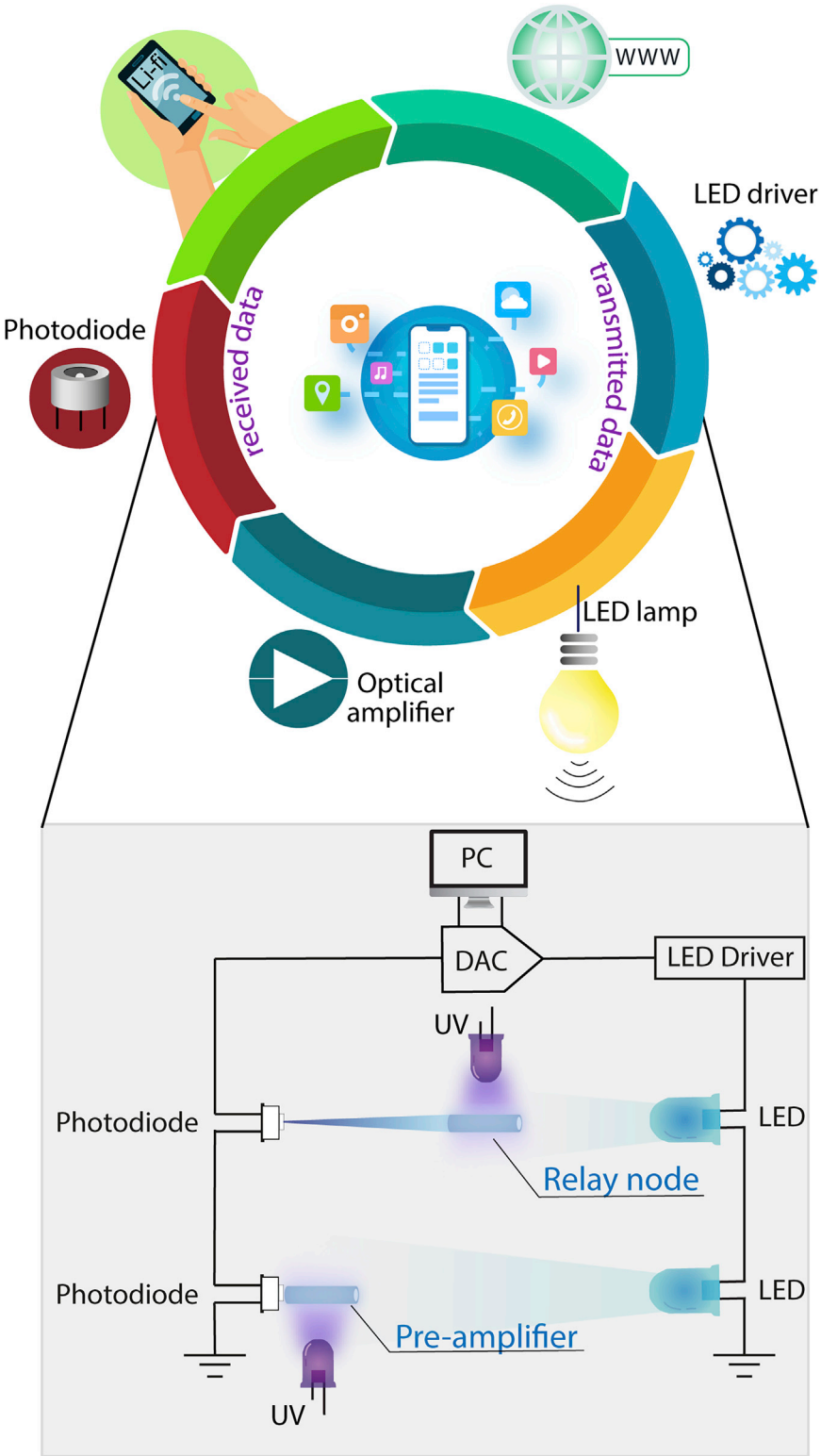


**Figure 1. Scheme of the VLC System**

Diagram of the proposed VLC system with optical amplification and the scheme of the experimental setup used for the transmission measurements in the VLC scenario using the fiber as a pre-amplifier and relay node.

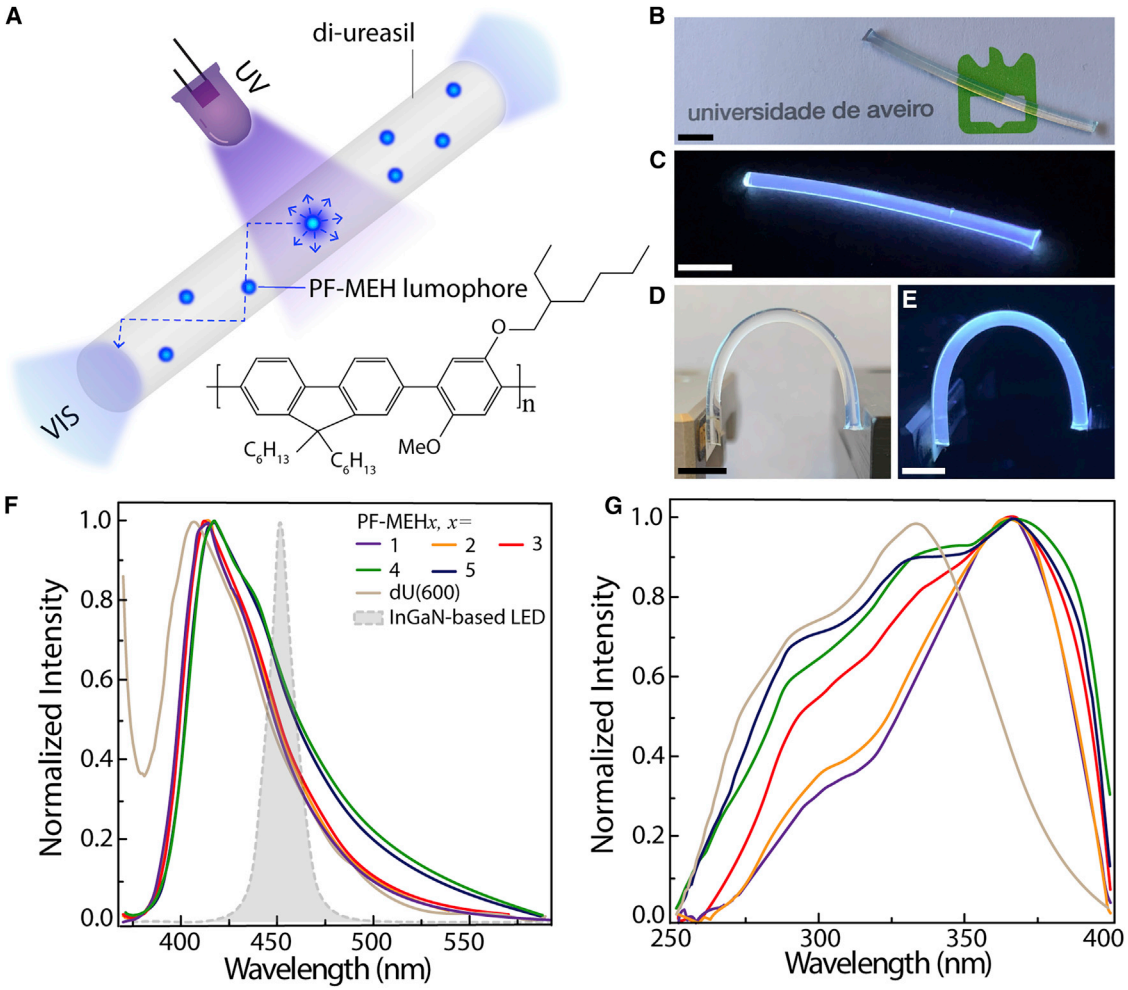


**Figure 2. Optical Properties of PF-MEH-Di-Ureasil Cylindrical Fibers**

(A) Representative scheme of the PF-MEH-di-ureasil fibers. The chemical structure of the blue lumophore PF-MEH is shown. The arrows inside the fiber indicate the total internal reflection of the emitted light.

(B–E) Photographs of the flexible PF-MEH3 fiber under daylight (B and D) and UV illumination (C and E). The scale bars represent 0.5 cm.

(F and G) Emission spectra excited at 360 nm for the fiber samples (F) and the corresponding excitation spectra monitored at 410 nm (G). The gray area in (F) represents the typical emission of the commercial InGaN-based, blue-emitting LED used to produce commercial solid-state lighting LEDs.[54]

approaches, similar gain values were obtained for the same input powers for each sample, showing the huge potential of these materials to be applied for both pre- or line amplification purposes to improve the reliability of VLCs. To perform these experiments, the fibers were exposed to prolonged UV radiation, revealing no sign of photodegradation.

## Simulation Results

To analyze the feasibility of integrating the proposed optical amplifier in a VLC system, numerical simulations were carried out for a realistic environment (an office of $4 \times 4 \times 3$ $m^3$). In order to meet the light levels recommended by the European Standard Norm (EN 12464-1) for an office and studying rooms (300 lm/m),[2,55] the room was designed with four LEDs in the ceiling (2 m apart from each other; Figure 4A).

First, the received optical power distribution was simulated in a scenario without optical amplification and the spatial distribution of the achieved bit error ratio (BER)

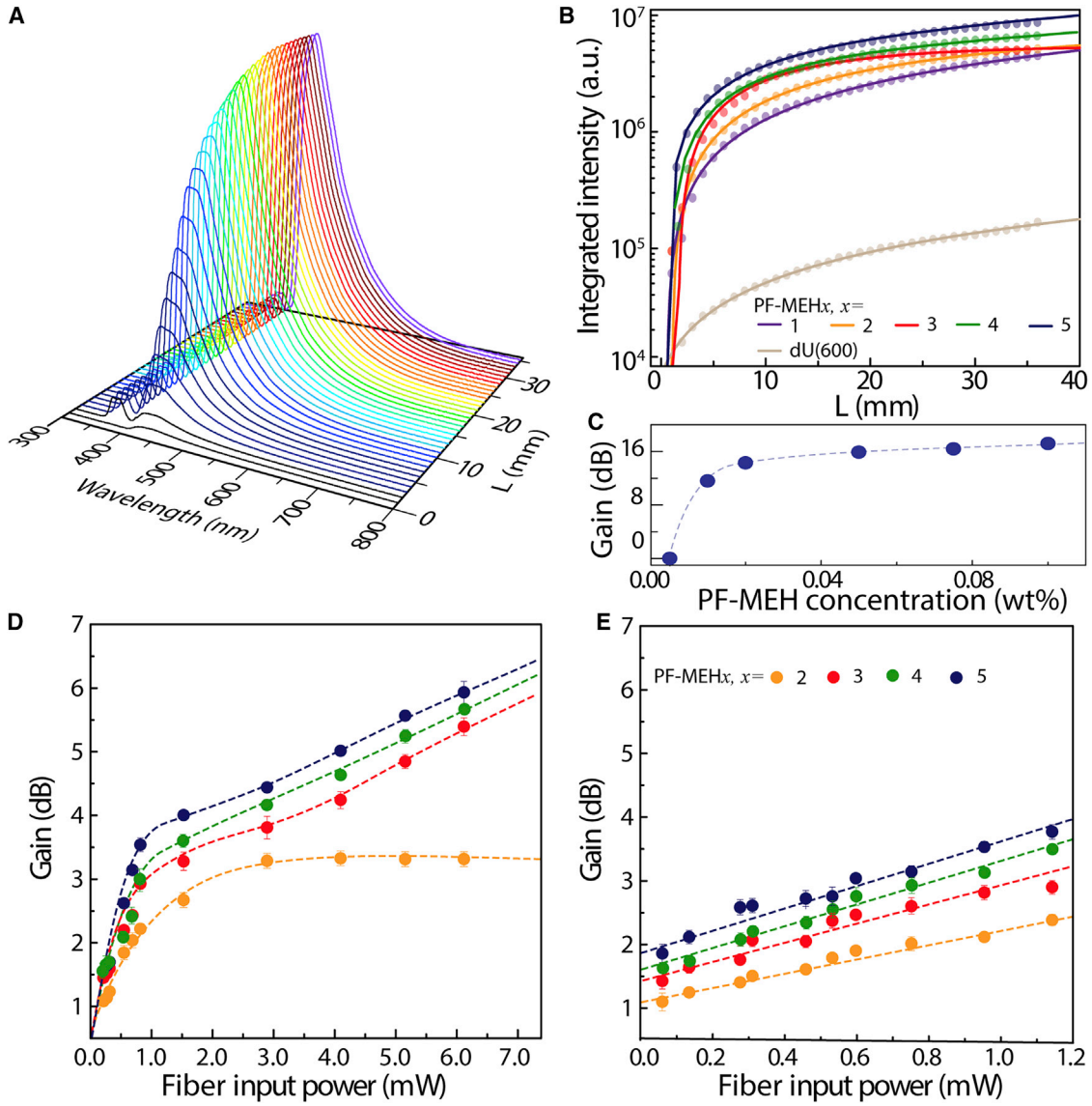


**Figure 3. Optical Gain of PF-MEH-Di-Ureasil Fibers Determined Using the Variable Stripe Method**

(A) Emission spectra of the PF-MEH fiber obtained for different stripe lengths (*L*).

(B) Integrated ASE intensities for all PF-MEH-di-ureasil samples as function of the stripe length.

(C) Calculated optical gain coefficients as a function of PF-MEH concentration (wt %) in the di-ureasil. The dashed line is a visual guide. Performance of PF-MEH-di-ureasil fibers as optical amplifiers in a VLC testbed is shown.

(D and E) Calculated optical gain as a function of the input power for the scenario where the fiber function as (D) a pre-amplifier and (E) a relay node. The data in (D) and (E) are represented as mean ± SEM.

was estimated, as shown in Figure 4B, showing a 2D joint Gaussian distribution with a full-width at half-maximum (FWHM) of 1.2 ± 0.1 m, centered with the LED location. The minimum BER value attained was $7.4 \times 10^{-5}$. To quantify the transmission quality, a BER limit of $3.8 \times 10^{-3}$ (corresponding to the 7% hard-decision forward error correction [HD-FEC])[56] was considered as the threshold limit. As illustrated in Figure 4B, the system is able to operate below this limit (region below the gray plane) and corresponds to 27% of the total room area. To improve the signal transmission (i.e., increase the area with a BER below the HD-FEC limit), we propose to amplify the optical signal using two different approaches: (1) pre-amplifier and (2) relay node. In

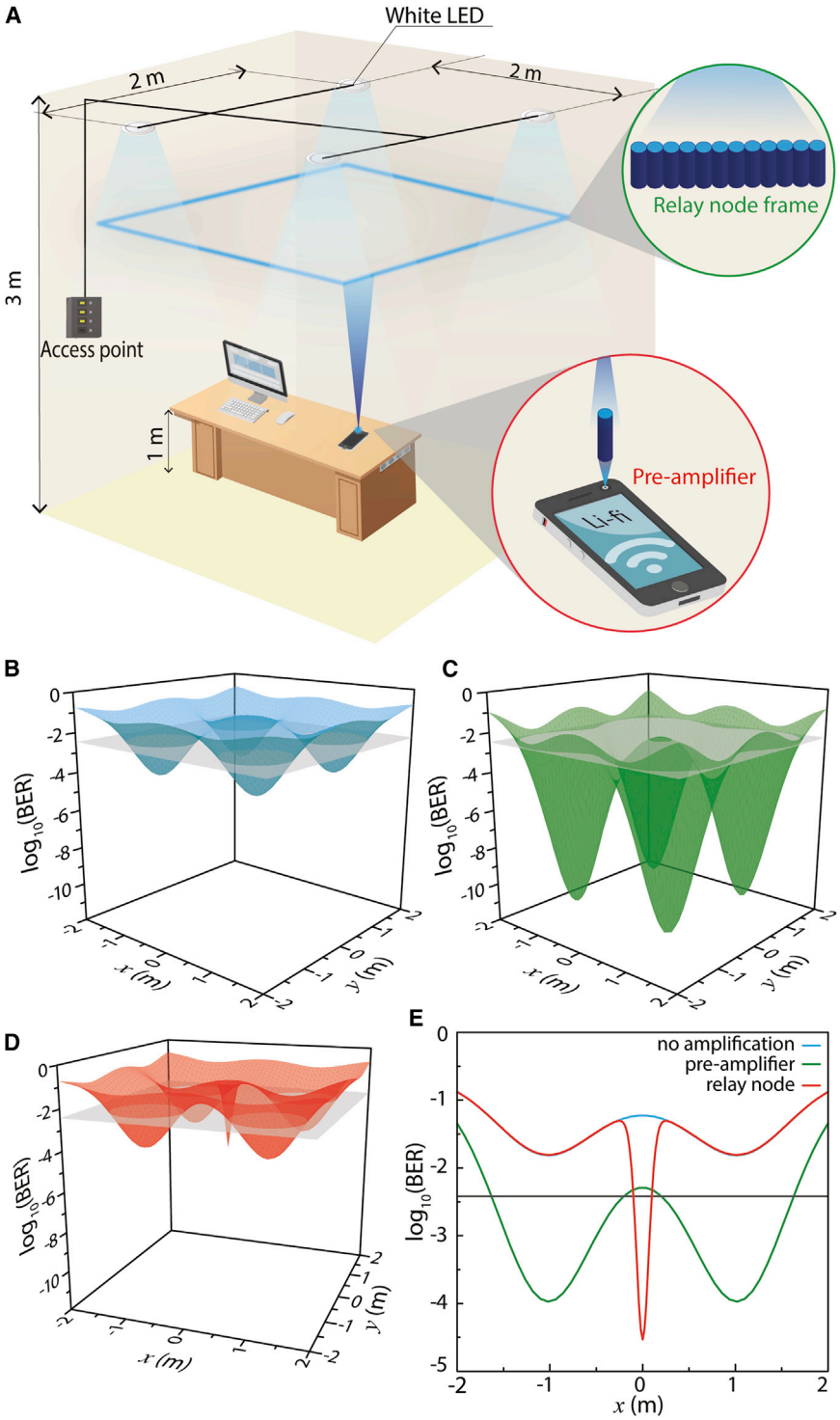


**Figure 4. Simulation of Optical Amplifier Performance in a Real-Life VLC Scenario**

(A) Scheme of the simulated indoor environment for the communication system.

(B–D) Simulated spatial distribution of BER: (B) without optical amplification and (C) with a pre-amplifier and (D) relay node. The gray area corresponds to the BER limit ($3.8 \times 10^{-3}$).

(E) BER profile for the above-mentioned scenarios along a cross-section in the middle of the room ($y = 0$ m).

the first approach, the optical amplifier is coupled to the photodiode and has a cylindrical shape whose base area is equal to the active area of the photodiode to optimize coupling. It was assumed that the fiber pre-amplifier has a gain of 5 dB and a length of 3.5 cm (as obtained experimentally). In this case, the BER of the received optical signal also presented a Gaussian distribution with a FWHM of 1.1 $\pm$ 0.6 m but with a minimum BER value of $2.6 \times 10^{-12}$ (Figure 4C). With this solution, an area of 13.1 $m^2$ can operate within the BER limit, which represents an increase of 207%. Nonetheless, this system cannot compensate the weaker signal in the middle of the room. A relay node was then implemented to improve this region. To model the relay node to form a frame of $2 \times 2$ $m^2$ with the vertices aligned with the LEDs, a group of $\approx$5,300 optical fiber amplifiers (maximum value to fill the frame) were assembled and placed between the LED and photodiode (1 m distance from each component). This scheme was chosen to simulate a window, where it is possible to incorporate the fibers in the frame. As the communication performance is weaker in the middle of the room, a lens was coupled to each fiber output to focus the amplified signal in that region. Figure 4D presents the distribution of the BER of the received signal, which shows an increase of 0.52% in the area able to operate below the BER limit, which corresponds to the area where the communication was weaker (Figure 4E). Therefore, the relay node can be added to complement the pre-amplification system, leading to an improvement in the VLC performance in the entire room and demonstrating the reliability of the proposed solution to improve VLC systems.

## DISCUSSION

We have demonstrated that monolithic flexible fibers based on the PF-MEH lumophore doped within a di-ureasil organic-inorganic hybrid host show significant potential as optical amplifiers in the visible spectral region for VLCs. Optical amplification using the PF-MEH-di-ureasil fibers was successfully demonstrated for both pre-amplifier and relay node scenarios in a VLC system, yielding high optical gains. To the best of our knowledge, this is the first time that an optical amplifier in the blue spectral region (390–550 nm) is implemented in a VLC system. It was also shown that, by controlling the lumophore loading (0–0.10 wt %), it is possible to tune the PL quantum yield (25%–52%) and the gain coefficient (3.3–4.9 dB/cm). The numerical simulation carried out for the system operation in a real-life environment, with a bit rate of 5 kbit/s, demonstrated that the incorporation of fiber optical amplifier could lead to a 207% increase of the room area with reliable communication using pre-amplification. Additionally, in the center of room, where the communication efficiency is weaker, there is a clear improvement of the BER values using the relay node scenario.

In summary, we demonstrated for the first time the use of optical amplification in the VLC context, improving the operational power budget, which is one of the main challenges to upgrade VLC. We present the most efficient (5.9 dB) organic-inorganic-based material reported so far for optical amplification, with additional advantages, such as mechanical flexibility, thermal stability, and low-cost and energy-efficient processing. The real application potential of this optical amplifier was unequivocally demonstrated in a VLC testbed and modeled through numerical simulations, showing an improvement in the communication efficiency and range using commercial devices (LEDs and photodetector). As far as we know, there are no solutions based on optical amplification to improve VLC performance, showing the huge potential of these compact and cost-effective fiber amplifiers to solve

this technological gap, which could play a fundamental role in the next generation of indoor lighting in green smart houses.

## EXPERIMENTAL PROCEDURES

### Materials

*Bis*(2-aminopropyl) polypropylene glycol-*block*-polyethylene glycol-*block*-polypropylene glycol (Jeffamine ED-600; $M_w$ = 600 g mol$^{-1}$) and 3-(triethoxysilyl)propylisocyanate (ICPTES; 95.0%) were purchased from Sigma-Aldrich. Tetrahydrofuran (THF) (≥99.9%), ethanol (EtOH) (95.0%), and hydrochloric acid (HCl) (37%) were purchased from Fisher Scientific. Water was obtained from Millipore Simpak 2 water purification system. Poly[(9,9-dihexylfluorenyl-2,7-diyl)-*alt*-*co*-(2-methoxy-5-{2-ethylhexyloxy}-1,4-phenylene)] (trade name ADS136BE, referred to here as PF-MEH; $M_n$ = 17,000 g mol$^{-1}$; Đ = 5.5) was purchased from American Dye Source. All materials were used as received.

### Synthesis and Processing of PF-MEH-Di-Ureasil Fibers

Fiber optical amplifiers based on the di-ureasil waveguide (denoted dU(600)) were prepared via a two-step sol-gel process. In the first step, ICPTES (0.91 mL; 3.68 mmol) was mixed with Jeffamine ED-600 (1.00 mL; 1.75 mmol) in THF (5 mL). The reaction mixture was refluxed at 70°C for 24 h to obtain "one batch" of the organic-inorganic hybrid precursor, diureapropyltriethoxysilane (d-UPTES). In the second step, gelling reagents (ethanol, HCl [0.5 M], and water, with a molar ratio of ICPTES: EtOH: HCl: $H_2O$ was 176: 350: 1: 265) were added to the d-UPTES in sequence and mixed vigorously. The resulting mixture (0.1 batch) was transferred into a polytetrafluoroethylene (PTFE) tube (internal diameter = 2.7 mm; length = 10 cm), and the ends of the tube were sealed with Teflon tape to allow slow evaporation of the THF as the sample was aged at room temperature over 7 days. The sample (still within the PTFE tube) was then oven dried at 40°C for 3 days. Following removal from the tube, the sample was obtained as a free-standing flexible fiber with a diameter of ~1.3 mm.

PF-MEH-doped di-ureasils were prepared by introducing a known volume of PF-MEH stock solution (1 mg mL$^{-1}$ in THF) into the d-UPTES precursor solution, prior to the addition of gelling reagents. The required volume was based on the lumophore loading required in the final sample (0.01, 0.02, 0.05, 0.075, and 0.1 wt % with respect to the mass of the dry monolith, where one batch of d-UPTES yields a dry monolith of 1.76 g). The stock solution of PF-MEH was pre-stirred for 48 h before use to ensure complete dissolution in the THF solvent. Samples are designated as PF-MEH*x*, where *x* equal to 1 is the least concentrated sample and 5 is the most concentrated sample (see Table S1; Supplemental Information).

### Photoluminescence Spectroscopy

Room temperature emission and excitation spectra were measured on a Fluorolog-3 spectrophotometer (Horiba Jobin Yvon) in the front-face configuration. Excitation and emission slits were adjusted so that the maximum PL intensity was within the range of linear response of the detector. Emission and excitation spectra were corrected for the wavelength response of the system and the intensity of the lamp profile over the excitation range, respectively, using correction factors supplied by the manufacturer.

### Absolute Emission Quantum Yield

The PL quantum yield values ($\phi$) were measured at room temperature using a Quantaurus-QY Plus C13534, Hamamatsu. The method is accurate within $\Delta\phi/\phi$ = 0.10.

### Variable Stripe Length Gain Measurement

The optical gain was measured using the variable stripe length method.[53] The sample was optically excited, and the amplified spontaneous emission signal intensity ($I_{ASE}$) was collected from the edge of the sample as a function of the length of the sample that was excited ($L$).[42] In order to excite the sample with a variable stripe length, a movable shutter connected to a translation stage was used, allowing the length to be controlled within the limits $0 \leq L \leq 35$ mm with a step of 1 mm. To detect the amplified spontaneous emission signal, an optical fiber and a spectrometer (MAYA Pro 2000; OceansOptics) were used with an integration time of 0.1 s. Excitation was performed with a UV lamp (Vilber VL-6.LC) emitting at 365 nm with a power density of $2.40 \pm 0.02$ W/cm$^2$.

### VLC Testbed Scenario

The data transmission tests were performed on a VLC system based on a commercial LED lamp (Codex-E Lamp; Lightenjin) acting as illumination and data source simultaneously. To quantify the LED lamp power, its spectral radiant flux (or spectral radiant power, W·nm$^{-1}$) was measured through an integrating sphere (ISP 150L-131; Instrument Systems) with a $BaSO_4$ coating and an internal diameter of 150 mm coupled to an array spectrometer (MAS-40; Instrument Systems). Before the measurements, a self-absorption correction was implemented using a reference lamp (ISP 150L-131; Instrument Systems).

The data sequence transmitted by the LED lamp was a binary message, generated in MATLAB, with a word length of $2^{13}$ bits, a bit rate of 200 bit/s, and a sampling rate of $10^5$ samples/s. The low bitrate was used only to simplify the experimental setup.

The digital message was converted to the analog domain by an ADALM1000 board (Analog Devices) and used to modulate in amplitude shift key the LED through a current source (T-Cube LED Driver; Thorlabs). Two different approaches were demonstrated: (1) a pre-amplifier and (2) in-line amplifier, which can be used as relay node. In the first approach, at the receiver, the fiber amplifier output was coupled into the photodiode active area (DET210; Thorlabs) with an index matching gel (G608N; Thorlabs). These transmission tests were performed with different distances between the transmitter and the receiver ($0.10 \leq L \leq 1.35$ m). In the second approach, the fiber amplifier was placed between the LED (25-cm distance) and the photodiode (7.5-cm distance), with a lens coupled into the fiber amplifier output, focusing the optical signal into the photodiode active area. The distance between the fiber output and the photodiode was imposed by the focal distance of the lens. The transmission tests were performed with different fiber input powers. In both approaches, the fiber amplifier was externally excited with an UV pump (VL-6.LC; Vilber) in a perpendicular pumping architecture. The photocurrent produced by the photodiode was also acquired with the ADALM1000 board, and the signal amplitude, BER, and signal-to-noise ratio (SNR) were obtained. Five independent measurements were taken, and the average of these measurements was used to estimate the optical gain in the fibers that presented the highest optical gain (PF-MEH2–PF-MEH5).

### VLC Scenario Simulation

To analyze the feasibility of the proposed VLC system integrating an optical amplifier, numerical simulations were carried out in MATLAB for a realistic environment (Figure 4A). Each LED transmits in amplitude-shift keying (ASK) modulation, with a modulation index of 100%, bit rate of 5 kbit/s, and a word length of $2^{15}$ bits. The respective signal amplitude was mapped with a spatial resolution of 2 cm on a

surface at 1-m height from the ground (typical value for office desks). The transmission channel was considered as line of sight, where the path between the transmitter and receiver is not interrupted.[32] In this model, the LED behaves as a *Lambert* radiator, which has a constant luminance in all directions, albeit with different luminous intensity levels, as depicted in Figure S3.[57] The luminous intensity ($I$) distribution function is expressed as

$$I(\phi) = I(0)\cos^m\phi, \quad \text{(Equation 1)}$$

where $\phi$ is the incident angle, $I(0)$ is the axial luminous intensity, and $m$ is the Lambertian order given by

$$m = -\frac{\ln 2}{\ln(\cos\phi_{1/2})}, \quad \text{(Equation 2)}$$

where $\phi_{1/2}$ is the half-power semi-angle (Figure S3).[57] In order to map the signal intensity at each point, defined by $X$ and $Y$, which are the coordinates for the $i$ axis and $j$ axis, respectively, the $\phi$ angle is given by Equation 3.

$$\phi = \arctan\left(\frac{\sqrt{X^2+Y^2}}{Z}\right), \quad \text{(Equation 3)}$$

where $Z$ is the coordinate for the $k$ axis. Relating $I(0)$ to the LED optical power ($P$), the signal intensity ($I$) can be given by Equation 4.

$$I(\phi) = \frac{P}{A_s}cos^m(\phi), \quad \text{(Equation 4)}$$

where $A_s$ is the photodiode active area.

After the transmission channel, the signal was analyzed and the constellation diagram was plotted for each point of the room with the above-mentioned spatial resolution. The BER values of the signal for all configurations were estimated based on the SNR value, through Equation 5, assuming an ASK modulation.

$$BER = \frac{1}{2}erfc\left(\sqrt{\frac{SNR}{4}}\right) \quad \text{(Equation 5)}$$

## DATA AND CODE AVAILABILITY

The authors declare that data supporting the findings of this study are available within the paper and the Supplemental Information. All other data are available from the lead contact upon reasonable request.

## SUPPLEMENTAL INFORMATION

Supplemental Information can be found online at https://doi.org/10.1016/j.xcrp.2020.100041.

## ACKNOWLEDGMENTS

This work was developed within the scope of the project CICECO-Aveiro Institute of Materials (UIDB/50011/2020 and UIDP/50011/2020), Instituto de Telecomunicações (UIDB/EEA/50008/2020), SusPhotoSolutions (CENTRO-01-0145-FEDER000005), and WINLEDs (POCI-01-0145-FEDER-030351), financed by national funds through the FCT/MEC and, when appropriate, co-financed by FEDER under the PT2020 Partnership Agreement through European Regional Development Fund (ERDF) in the frame of Operational Competitiveness and Internationalization Programme (POCI). The authors thank V.T. Freitas from the Lightenjin Company for supplying the LED lamp and Prof. L.D. Carlos from the University of Aveiro for thoughtful

insight into the discussion of the results presented. T.S. thanks the grant financed by the SOLARFLEX project (CENTRO-01-0145-FEDER-030186). R.C.E. acknowledges funding from the European Research Council (ERC) under the European Union's Horizon 2020 research and innovation programme (grant agreement no. 818762 - SPECTRACON).

## AUTHOR CONTRIBUTIONS

A.R.B. and T.S. designed the experiments for the optical characterization measurements, VLC testbed measurements, and simulations. R.C.E. and R.A.S.F. interpreted the photoluminescence data, and P.S.A. discussed the optical properties and the simulation results. G.L. and R.C.E synthesized the PF-MEH doped within a di-ureasil organic-inorganic hybrid. P.S.A. conceived the application for VLC. P.S.A., R.C.E., and R.A.S.F. conceived the approach and supervised the work.

## DECLARATION OF INTERESTS

The authors declare no competing interests.

Received: January 21, 2020
Revised: February 18, 2020
Accepted: February 20, 2020
Published: April 22, 2020

## REFERENCES

1. Sewaiwar, A., Tiwari, S.V., and Chung, Y.H. (2015). Smart LED allocation scheme for efficient multiuser visible light communication networks. Opt. Express *23*, 13015–13024.
2. Tiwari, S.V., Sewaiwar, A., and Chung, Y.-H. (2015). Smart home technologies using visible light communication. 2015 IEEE International Conference on Consumer Electronics (IEEE), pp. 379–380.
3. Chi, Y.C., Huang, Y.F., Wu, T.C., Tsai, C.T., Chen, L.Y., Kuo, H.C., and Lin, G.R. (2017). Violet laser diode enables lighting communication. Sci. Rep. *7*, 10469.
4. Haas, H., Chen, C., and O'Brien, D. (2017). A guide to wireless networking by light. Prog. Quantum Electron. *55*, 88–111.
5. Wang, W.C., Wang, H.Y., and Lin, G.R. (2018). Ultrahigh-speed violet laser diode based free-space optical communication beyond 25 Gbit/s. Sci. Rep. *8*, 13142.
6. FCC (2019). Table of frequency allocations chart. (FCC).
7. Grobe, L., Paraskevopoulos, A., Hilt, J., Schulz, D., Lassak, F., Hartlieb, F., Kottke, C., Jungnickel, V., and Langer, K.-D. (2013). High-speed visible light communication systems. IEEE Commun. Mag. *51*, 60–66.
8. Chow, C.-W., Yeh, C.-H., Liu, Y.-F., and Huang, P.Y. (2013). Mitigation of optical background noise in light-emitting diode (LED) optical wireless communication systems. IEEE Photonics J. *5*, 7900307.
9. Elgala, H., Mesleh, R., and Haas, H. (2011). Indoor optical wireless communication: potential and state-of-the-art. IEEE Commun. Mag. *49*, 56–62.
10. Kavehrad, M. (2010). Sustainable energy-efficient wireless applications using light. IEEE Commun. Mag. *48*, 66–73.
12. Chi, Y.C., Hsieh, D.H., Lin, C.Y., Chen, H.Y., Huang, C.Y., He, J.H., Ooi, B., DenBaars, S.P., Nakamura, S., Kuo, H.C., and Lin, G.R. (2015). Phosphorous diffuser diverged blue laser diode for indoor lighting and communication. Sci. Rep. *5*, 18690.
13. Rawat, B.S., Aggarwal, B., and Passi, D. (2014). Li-Fi: a new era of wireless communication data sharing. Int. J. Sci. Technol. Res. *3*, 118–119.
14. Wu, T.C., Chi, Y.C., Wang, H.Y., Tsai, C.T., Huang, Y.F., and Lin, G.R. (2017). Tricolor R/G/B laser diode based eye-safe white lighting communication beyond 8 Gbit/s. Sci. Rep. *7*, 11.
15. Chi, Y.C., Hsieh, D.H., Tsai, C.T., Chen, H.Y., Kuo, H.C., and Lin, G.R. (2015). 450-nm GaN laser diode enables high-speed visible light communication with 9-Gbps QAM-OFDM. Opt. Express *23*, 13051–13059.
16. Khan, L.U. (2017). Visible light communication: applications, architecture, standardization and research challenges. Dig. Commun. Netw. *3*, 78–88.
17. UN (2019). The Sustainable Development Goals Report (United Nations).
18. Cisco (2019). Cisco Visual Networking Index: Global Mobile Data Traffic Forecast Update, 2017–2022 White Paper (Cisco).
19. Kim, H.-S., Kim, D.-R., Yang, S.-H., Son, Y.-H., and Han, S.-K. (2013). An indoor visible light communication positioning system using a RF carrier allocation technique. J. Lightwave Technol. *31*, 134–144.
20. Liang, Q. (2015). Ford and NTU Tie up in VLC Project to Enhance Driving Safety (Taiwan Sourcing Service Provider).
21. Cui, K., Chen, G., Xu, Z., and Roberts, R.D. (2012). Traffic light to vehicle visible light communication channel characterization. Appl. Opt. *51*, 6594–6605.
22. Wu, T.C., Chi, Y.C., Wang, H.Y., Tsai, C.T., and Lin, G.R. (2017). Blue laser diode enables underwater communication at 12.4 Gbps. Sci. Rep. *7*, 40480.
23. Huang, Y.-F., Tsai, C.-T., Chi, Y.-C., Huang, D.-W., and Lin, G.-R. (2018). Filtered multicarrier OFDM encoding on blue laser diode for 14.8-Gbps seawater transmission. J. Lightwave Technol. *36*, 1739–1745.
24. Muhammad, S., Qasid, S.H.A., Rehman, S., and Rai, A.B. (2016). Visible light communication applications in healthcare. Technol. Health Care *24*, 135–138.
25. Song, J., Ding, W., Yang, F., Yang, H., Wang, J., Wang, X., and Zhang, X. (2014). Indoor Hospital Communication Systems: An Integrated Solution Based on Power Line and Visible Light Communication. 2014 IEEE Faible Tension Faible Consommation (IEEE).
26. Claudel, E., Fouassier, E., and Lopez, J. (2014). Wireless partitioned on-board telecommunication network. US patent US9596142B2, filed June 13, 2014, and published March 14, 2017.
27. Grand View Research (2016). Visible Light Communication/Light Fidelity Market Worth $101.30 Billion By 2024. https://www.grandviewresearch.com/press-release/global-visible-light-communication-market.

28. Dhamodaran, S., Afridi, M., Rahul, M., Refonaa, J., and Ashok Kumar, K. (2019). Retail store evoluvation between customer–vendor using Li-Fi technology. J. Comput. Theor. Nanosci. *16*, 3316–3318.

29. Pust, P., Schmidt, P.J., and Schnick, W. (2015). A revolution in lighting. Nat. Mater. *14*, 454–458.

30. de Almeida, A., Zissis, G., Quicheron, M., and Bertoldi, P. (2013). Accelerating the Deployment of Solid State Lighting (SSL) in Europe (European Union).

31. Pimputkar, S., Speck, J.S., DenBaars, S.P., and Nakamura, S. (2009). Prospects for LED lighting. Nat. Photonics *3*, 180–182.

32. Ghassemlooy, Z., Alves, L.N., Zvánovec, S., and Khalighi, M.-A. (2017). Visible Light Communications Theory and Applications (CRC).

33. Sebastián, J., Lamar, D.G., Aller, D.G., Rodríguez, J., and Miaja, P.F. (2018). On the role of power electronics in visible light communication. IEEE J. Em. Sel. Top. P. *6*, 1210–1223.

34. Mei, S., Liu, X., Zhang, W., Liu, R., Zheng, L., Guo, R., and Tian, P. (2018). High-bandwidth white-light system combining a micro-LED with perovskite quantum dots for visible light communication. ACS Appl. Mater. Interfaces *10*, 5641–5648.

35. Dursun, I., Shen, C., Parida, M.R., Pan, J., Sarmah, S.P., Priante, D., Alyami, N., Liu, J., Saidaminov, M.I., et al. (2016). Perovskite nanocrystals as a color converter for visible light communication. ACS Photonics *3*, 1150–1156.

36. Sajjad, M.T., Manousiadis, P.P., Orofino, C., Kanibolotsky, A.L., Findlay, N.J., Rajbhandari, S., Vithanage, D.A., Chun, H., Faulkner, G.E., O'Brien, D.C., et al. (2017). A saturated red color converter for visible light communication using a blend of star-shaped organic semiconductors. Appl. Phys. Lett. *110*, 013302.

37. Fuada, S., Putra, A.P., Aska, Y., and Adiono, T. (2016). Trans-impedance amplifier (HA) design for visible light communication (VLC) using commercially available OP-AMP. 2016 3rd International Conference on Information Technology, Computer, and Electrical Engineering (ICITACEE) (IEEE), pp. 31–35.

38. Li, X., Hussain, B., Wang, L., Jiang, J., and Yue, C.P. (2018). Design of a 2.2-mW 24-Mb/s CMOS VLC receiver SoC with ambient light rejection and post-equalization for Li-Fi applications. J. Lightwave Technol. *36*, 2366–2375.

39. Forrest, S.R. (2004). The path to ubiquitous and low-cost organic electronic appliances on plastic. Nature *428*, 911–918.

40. Chun, H., Rajbhandari, S., Faulkner, G., and O'Brien, D. (2014). Effectiveness of blue-filtering in WLED based indoor visible light communication. 2014 3rd International Workshop in Optical Wireless Communications (IWOW) (IEEE), pp. 60–64.

41. Bastos, A., McKenna, B., Silvério, T., Carlos, L.D., André, P.S., Carlos, L.D., Evans, R.C., and Ferreira, R.A.S. (2019). Innovative and multifunctional materials as optical amplifiers for cooperative visible light communications, 2019 18th SBMO/IEEE MTT-S International Microwave and Optoelectronics Conference (IMOC) (IEEE).

42. Bastos, A., McKenna, B., Lima, M., André, P.S., Carlos, L.D., Evans, R.C., and Ferreira, R.A.S. (2018). Flexible optical amplifier for visible-light communications based on organic-inorganic hybrids. ACS Omega *3*, 13772–13781.

43. Evans, R.C. (2013). Harnessing self-assembly strategies for the rational design of conjugated polymer based materials. J. Mater. Chem. C *1*, 4190–4200.

44. Willis-Fox, N., Marques, A.T., Arlt, J., Scherf, U., Carlos, L.D., Burrows, H.D., and Evans, R.C. (2015). Synergistic photoluminescence enhancement in conjugated polymer-di-ureasil organic-inorganic composites. Chem. Sci. (Camb.) *6*, 7227–7237.

45. Willis-Fox, N., Kraft, M., Arlt, J., Scherf, U., and Evans, R.C. (2016). Tunable white-light emission from conjugated polymer-di-ureasil materials. Adv. Funct. Mater. *26*, 532–542.

46. Lima, P.P., Sá Ferreira, R.A., Freire, R.O., Almeida Paz, F.A., Fu, L., Alves, S., Jr., Carlos, L.D., and Malta, O.L. (2006). Spectroscopic study of a UV-photostable organic-inorganic hybrids incorporating an Eu3+ beta-diketonate complex. ChemPhysChem *7*, 735–746.

47. Fu, L., Sá Ferreira, R.A., Fernandes, M., Nunes, S.C., de Zea Bermudez, V., Hungerford, G., Rocha, J., and Carlos, L.D. (2008). Photoluminescence and quantum yields of organic/inorganic hybrids prepared through formic acid solvolysis. Opt. Mater. *30*, 1058–1064.

48. Ferreira, R.A.S., Brites, C.D.S., Vicente, C.M.S., Lima, P.P., Bastos, A.R.N., Marques, P.G., Hiltunen, M., Carlos, L.D., and André, P.S. (2013). Photonic-on-a-chip: a thermal actuated Mach-Zehnder interferometer and a molecular thermometer based on a single di-ureasil organic-inorganic hybrid. Laser Photonics Rev. *7*, 1027–1035.

49. Schlereth, T.W., Schneider, C., Kaiser, W., Höfling, S., and Forchel, A. (2007). Low threshold, high gain AlGaInAs quantum dot lasers. Appl. Phys. Lett. *90*, 221113.

50. George, N.C., Denault, K.A., and Seshadri, R. (2013). Phosphors for solid-state white lighting. Annu. Rev. Mater. Res. *43*, 481–501.

51. Carlos, L.D., de Zea Bermudez, V., Sá Ferreira, R.A., Marques, L., and Assunção, M. (1999). Sol−gel derived urea cross-linked organically modified silicates. 2. Blue-light emission. Chem. Mater. *11*, 581–588.

52. Li, Y., Dvořák, M., Nesterenko, P.N., Nuchtavorn, N., and Macka, M. (2018). High power deep UV-LEDs for analytical optical instrumentation. Sens. Actuators B Chem. *255*, 1238–1243.

53. Dal Negro, L., Bettotti, P., Cazzanelli, M., Pacifici, D., and Pavesi, L. (2004). Applicability conditions and experimental analysis of the variable stripe length method for gain measurements. Opt. Commun. *229*, 337–348.

54. Wu, H., Zhang, X., Guo, C., Xu, J., Wu, M., and Su, Q. (2005). Three-band white light from InGaN-based blue LED chip precoated with green/red phosphors. IEEE Photonics Technol. Lett. *17*, 1160–1162.

55. BSI (2011). Light and Lighting—Lighting of Work Places. Part 1: Indoor Work Places (BSI).

56. Chang, F., Onohara, K., and Mizuochi, T. (2010). Forward error correction for 100 G transport networks. IEEE Commun. Mag. *48*, S48–S55.

57. Qiu, Y., Chen, H.-H., and Meng, W.-X. (2016). Channel modeling for visible light communications—a survey. Wirel. Commun. Mob. Comput. *16*, 2016–2034.